doi:10.1016/j.jmb.2008.09.062 J. Mol. Biol. (2008) 384, 718–729

JMB

Available online at www.sciencedirect.com

ScienceDirect

ELSEVIER

The Binding of Thioflavin T and Its Neutral Analog BTA-1 to Protofibrils of the Alzheimer's Disease $A\beta_{16–22}$ Peptide Probed by Molecular Dynamics Simulations

Chun Wu[1,2], Zhixiang Wang[3], Hongxing Lei[4], Yong Duan[5,6], Michael T. Bowers[1,2] and Joan-Emma Shea[1,2]*

[1]*Department of Chemistry and Biochemistry, University of California, Santa Barbara, CA 93106, USA*

[2]*Department of Physics, University of California, Santa Barbara, CA 93106, USA*

[3]*College of Chemistry and Chemical Engineering, Graduate University, Chinese Academy of Science, Beijing, China*

[4]*Beijing Institute of Genomics, Chinese Academy of Science, Beijing, China*

[5]*UC Davis Genome Center, University of California, Davis, CA 95616, USA*

[6]*Department of Applied Science, University of California, Davis, CA 95616, USA*

Received 30 June 2008; received in revised form 18 September 2008; accepted 23 September 2008
Available online 7 October 2008

Edited by D. Case

Thioflavin T (ThT) is a fluorescent dye commonly used to stain amyloid plaques, but the binding sites of this dye onto fibrils are poorly characterized. We present molecular dynamics simulations of the binding of ThT and its neutral analog BTA-1 [2-(4′-methylaminophenyl)benzothiazole] to model protofibrils of the Alzheimer's disease $A\beta_{16–22}$ (amyloid β) peptide. Our simulations reveal two binding modes located at the grooves of the β-sheet surfaces and at the ends of the β-sheet. These simulations provide new insight into recent experimental work and allow us to characterize the high-capacity, micromolar-affinity site seen in experiment as binding to the β-sheet surface grooves and the low-capacity, nanomolar-affinity site seen as binding to the β-sheet extremities of the fibril. The structure–activity relationship upon mutating charged ThT to neutral BTA-1 in terms of increased lipophilicity and binding affinity was studied, with calculated solvation free energies and binding energies found to be in qualitative agreement with the experimental measurements.

Keywords: amyloid fibrils; Alzheimer's disease $A\beta_{16–22}$ peptide; aggregation; thioflavin T; molecular dynamics simulations

Introduction

Amyloidoses are a class of diseases characterized by the pathological deposition of protein aggregates in the form of amyloid plaques on organs and tissues in the body. Huntington's disease, Parkinson's disease, type II diabetes, and Alzheimer's disease are all examples of amyloid diseases.[1,2] While the precise causative agent of these diseases remains a matter of debate, it is well established that amyloidoses involve either the incorrect folding of proteins

*Corresponding author. Department of Chemistry and Biochemistry, University of California, Santa Barbara, CA 93106, USA. E-mail address: shea@chem.ucsb.edu.

Abbreviations used: ThT, thioflavin T; BTA-1, 2-(4′-methylaminophenyl)benzothiazole; Aβ, amyloid β; CR, Congo red; MM-GBSA, molecular mechanics generalized Born/surface area; TI, thermodynamic integration; AFM, atomic force microscopy; LJ, Lennard–Jones.

or the structuring of natively disordered peptides, followed by their self-assembly to protein/peptide aggregates. The aggregation process involves the formation of small soluble oligomers, protofibrils, and fibrils and, finally, their deposition as amyloid plaques. Fibrillar aggregates, regardless of the peptide or protein involved, have a generic structure, involving cross β-sheets in which cross-strand main-chain hydrogen bonds lay parallel with the fibril axis. From a biomedical standpoint, it is critical to have a means of identifying amyloid aggregates in order to diagnose amyloid diseases in patients and for the development of therapeutics. To date, one of the most common and powerful means of characterizing amyloid fibrils is through the use of fluorescent dyes, which include, among others, derivatives of Congo red (CR) and thioflavin T (ThT).[3] CR undergoes a metachromatic shift in its absorbance spectrum and ThT undergoes a change in its excitation spectrum in the presence of amyloid fibrils but not in the presence of amyloidogenic peptide or protein monomers. The spectrum change is believed to be due to the resulting change in chemical environment upon binding of the dye to the β-sheets of the fibril. While these dyes offer a reliable means of visualizing aggregates through staining, the current lack of available high-resolution structural information has left several open questions, including the nature of the molecular form in which the dye binds the fibril, the binding locations on the fibril, and the mechanism of fluorescence enhancement upon binding. Experiments by Krebs *et al.*[4] suggest that ThT binds in a monomeric form along the fibril axis in the regular grooves formed by the side chains of residues n and $n+2$ of the registered β-strands on the surface of the β-sheet of the fibril. In this model, steric interactions between dye molecules and the side chains of the fibril would be responsible for the fluorescence enhancement. Groenning *et al.*,[5,6] on the other hand, proposed that ThT binds as a dimer in the central pore of the fibril, along the fibril, or at the interface between the protofilaments composing the mature fibril. In this case, formation of an excimer would account for the fluorescence increase upon ThT binding. Finally, Khurana *et al.*[7] proposed that ThT binds to amyloid fibrils as a preformed micelle of about 3 nm in diameter and that the fluorescence enhancement is due to the hydrogen bonding of the micelle to the amyloid fibril. This latter model has recently been challenged by Sabate *et al.*,[8] who showed that the critical micelle concentration of ThT (~35 μM) is 1 order of magnitude greater than the concentrations used in typical staining experiments (<5 μM), intimating that ThT cannot bind as a preformed micelle. It is clear that obtaining a molecular level of understanding of binding is essential in order to interpret binding experiments as well as for the design of better dyes for clinical purposes.

The primary aim of this study was to theoretically investigate the binding of ThT and one of its neutral derivatives [BTA-1 (2-(4′-methylaminophenyl)benzothiazole)] to amyloid fibrils. We wished to determine where these dyes bind on the fibril and how mutating ThT to BTA-1 affects solubility and binding affinity. We focused on aggregates of the Alzheimer's disease Aβ (amyloid β) peptide implicated in the said disease for two reasons: (1) this system serves as a model case for the general class of amyloid aggregation and (2) much of the experimental work on amyloid imaging agents has involved this peptide. The Aβ peptide is a proteolytic byproduct of the enzymatic cleavage of the amyloid precursor protein and typically ranges from 39 to 42 residues in length, although shorter fragments have also been shown to aggregate into amyloid fibrils.[9–12] ThT (cationic benzothiazole aniline/$C_{17}H_{19}ClN_2S$), shown in Fig. 1, undergoes a characteristic 115-nm red shift of its excitation spectrum upon binding to Aβ (and other) amyloid fibrils.[13] To improve the ability of this dye to cross the brain–blood barrier, a necessity for *in vivo* studies, the lipophilicity of the dye was more than 600-fold by removing the positively charged quaternary heterocyclic nitrogen. Among the derivatives resulting from this substitution, the BTA-1 dye emerged as one of the more promising dyes, capable of binding to Aβ$_{40}$ fibrils with much higher affinity (K_i = 20.2 nM) compared with ThT (K_i = 890 nM).[14] A further variant (PIB) of BTA-1, a hydroxylated BTA-1 derivative, had brain clearance properties comparable with those of PET radiotracers[15] and was shown to be capable of detecting amyloid fibrils in humans.[16–23] Experimental binding studies of ThT and its derivatives onto Aβ fibrils have identified at least three sites, with different binding stoichiometries and affinities (Table 1).[25] These three sites can be grouped into two main types/modes based on their binding ratios and affinities: a high-capacity, micromolar-affinity site (type I) and a low-capacity, nanomolar-affinity site (type II). The two sites of type I appear to be located near each other and, based on fluorescence studies, to correspond to hydrophobic pockets on the Aβ fibril.[25] Detailed structural information of ThT binding at the atomic level is not available, and this hinders not only our understanding of binding mechanisms but also the design of better dyes for clinical purposes.

Here, we used molecular dynamics simulations to study the binding of ThT and BTA-1 to model fibrils of the Aβ$_{16–22}$ (sequence KLVFFAE) peptide. This 7-residue fragment encompasses the central hydrophobic core of the full-length Aβ peptide[22] and

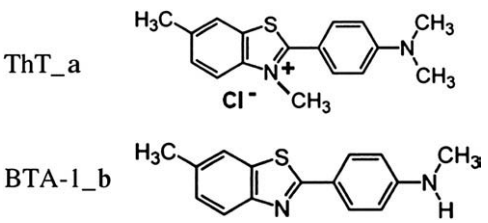

Fig. 1. Structures of two amyloid dyes. (a) ThT. (b) Neutral analog BTA-1.

Table 1. Summary of the three binding sites for the ThT class of amyloid dyes onto $A\beta_{40}$ fibrils seen in fluorescent experiments and in this simulation study

Proposed location[a]	Type Ia	Type Ib	Type II	Overall
	Grooves on β-sheet surface		Ends of β-sheet	
Ratio (ligand/peptide)	1:4	1:35	1:300	
ThT (K_d) (nM)	6000[b]	750	1610	580[c]
BTA-1 (K_d) (nM)	ND[d]	200	19.5	10[c]
Enhancement (ratio)	ND[d]	4	80	58

For fluorescent experiments, see Ref. 25.
[a] See Fig. 4.
[b] Ref. 24.
[c] Ref. 15.
[d] ND indicates not determined.

has been shown by solid-state NMR, electron microscopy, X-ray powder diffraction, and optical birefringence measurements with amyloid dyes (including ThT) to form highly ordered amyloid fibrils, consisting of β-sheets with in-register antiparallel β-strands in each β-sheet. Furthermore, in both $A\beta_{40}$[26,27] and $A\beta_{16–22}$[11,12] fibrils, the 16–22 KLVFFAE segment is in a β-strand configuration, with the requisite hydrophobic sites on the β-sheet surface available for type I binding. The small size of the $A\beta_{16–22}$ peptide makes it an ideal model system for theoretical studies of early oligomerization,[28–31] fibril formation,[32] and inhibition,[33] as well as the binding of dyes to amyloid aggregates. Our simulations enabled us to identify at an atomic level the binding sites for the dyes as well as the binding form of the dyes and to explain the binding stoichiometries from experiments. Our solvation free energy and binding energy analyses also shed light on the enhancement of lipophilicity and binding affinity arising from modifying ThT to BTA-1.

Results

We constructed a protofibril consisting of two parallel β-sheets, each composed of eight in-register antiparallel β-strands, as described in Materials and Methods. This $A\beta_{16–22}$ protofibril, shown in Fig. 2a, retained its two-layered β-sheet structure and was stable at 320 K over the course of all eight 20-ns ThT/protofibril and BTA-1/protofibril simulations, as indicated by the small root mean square deviation (RMSD = 1.7 ± 0.2 Å) from the starting structure. Reversible binding of dye to the protofibril was observed in trajectories (See Fig. S1 for a typical trajectory). At the end of the simulations (each simulation involved one protofibril and four dye molecules; see Materials and Methods), on average, three of four ThT dye molecules and all four BTA-1 dye molecules were stably bound to the protofibril (data not shown). While ThT bound the fibril as a monomer in all trajectories, BTA-1 formed a dimer in one trajectory through the stacking of a BTA-1 monomer on top of an already β-sheet surface-bound BTA-1 monomer. In the three other trajectories, BTA-1 bound as a monomer. The neutral BTA-1 molecule would appear to have a higher tendency to form oligomers than the positively charged ThT dyes. We note that the absence of dimers of ThT in our simulations does not preclude their existence: we may not see dimer formation because of the system size (i.e., a limited number of dye molecules present in our periodic box). We do not expect to see micelles in our simulation because the effective concentration in the simulations is in the range used in staining experiments (<5 μM), well below the critical micellar concentration (~35 μM).

To identify the binding sites of the dye, we superimposed the protofibril structure of the bound complexes identified from the trajectories (see Fig. 3). For ThT, four populated ligand clusters were identified: one cluster along the central straight groove [F4–; –F4] formed by the Phe rings on the surface of the lower sheet layer (Fig. 3a1), another cluster along the central kink groove [V3–F5; F5–V3] between the side chains of Val and Phe (this groove is due to the antiparallel arrangement of the β-strands in the upper sheet layer), and, finally, two clusters at two ends of the β-sheet. Because the two ends of the β-sheet are chemically equivalent, the last two clusters correspond to the same binding site. Thus, three binding sites are identified from the four clusters: two clusters parallel with the β-sheet extension (main-chain hydrogen bond) direction and one cluster parallel with the β-strand direction.

The binding patterns for BTA-1 are shown in Fig. 3b1 and 2. All three binding sites seen for ThT (Fig. 3a) were also observed for BTA-1. This is consistent

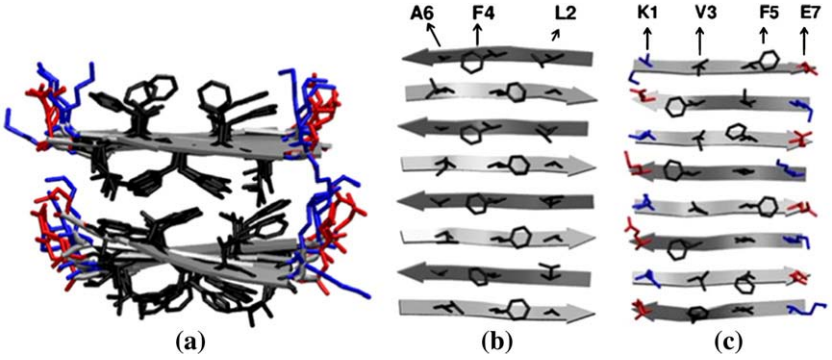

Fig. 2. $A\beta_{16–22}$ protofibril consisting of two β-sheets with eight in-register antiparallel β-strands in each β-sheet. (a) Two β-sheets stacked in parallel. (b) The grooves along the β-sheet extension direction, between the surface side chains on the surface of the lower sheet layer. (c) The grooves on the surface of the upper sheet layer. The positively charged, negatively charged, and hydrophobic side chains are shown in blue, red, and black, respectively.

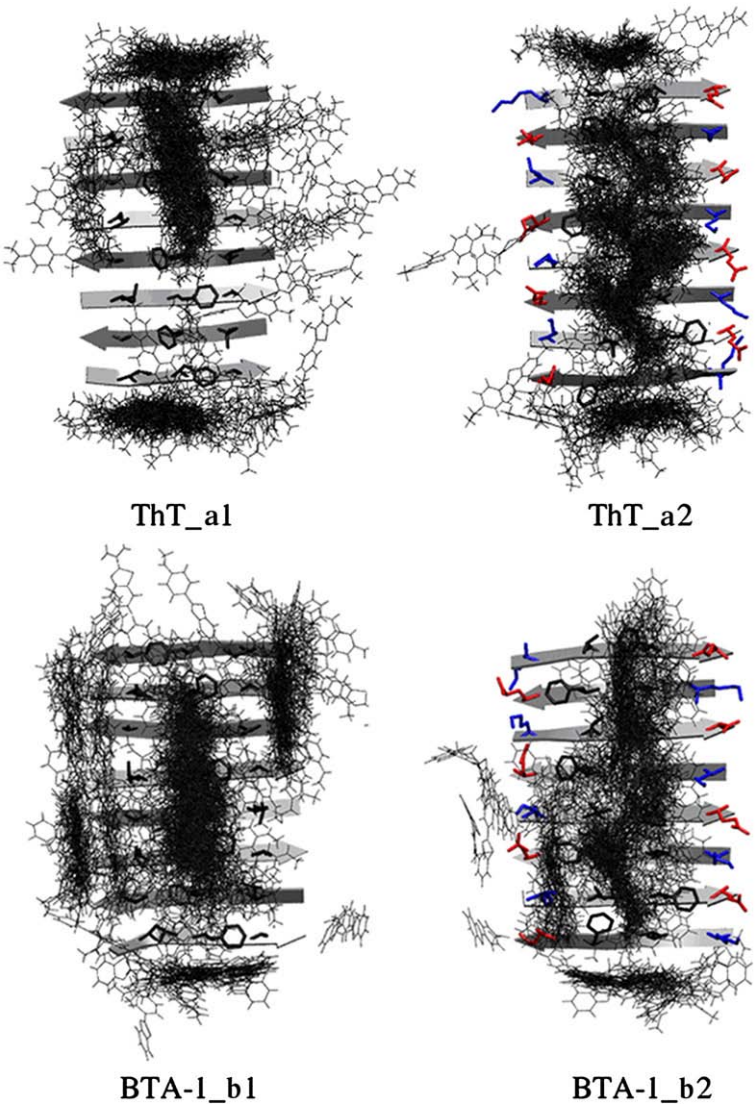

Fig. 3. Distribution of the bound dyes around the protofibril. Panels (a1) and (a2) show the binding of ThT, while panels (b1) and (b2) show the binding of BTA-1. In (a1) and (b1), binding is shown on the lower sheet layer. In (a2) and (b2), binding is shown on the upper sheet layer. Dyes are represented by lines; the positively charged, negatively charged, and hydrophobic side chains of the peptide are shown in blue, red, and black, respectively.

with the fact that the positively charged ThT molecules did not bind to the negatively charged E22, indicating that charge–charge interaction may not play a dominant role in recognizing the protofibril. Hence, removing the charge on ThT (as was done to create the neutral analog BTA-1) should not alter the binding at the three binding sites. However, the following differences emerged: (1) binding at the two ends of the β-sheet was reduced and (2) two additional bindings in the side grooves were observed on the surface of the two sheet layers ([L2–; A6–] of the lower sheet layer and [K1–V3; E7–F5] of the upper sheet layer). The latter may indicate that charge removal enhances the hydrophobic interaction between the dye and the protofibril, leading to additional binding in the side grooves.

A two-level clustering analysis was carried out, as described in Materials and Methods. For ThT, the top 15 clusters of the bound complex could be grouped into the three binding sites described earlier: binding in the central grooves of the lower sheet layer, binding in the central grooves of the upper sheet layer, and binding at the end of the β-sheet. For BTA-1, two more binding sites were again identified: the first involves binding in the side grooves of the lower sheet layer, and the second involves binding in the side grooves of the upper sheet layer. A representative complex structure at each site and its abundance are shown in Fig. 4.

For both ThT and BTA-1, binding in the grooves (including the side grooves for BTA-1) of the sheet layers appears to be more favorable than binding at the two ends, as indicated by the larger abundance seen in the clustering studies shown in Fig. 4 (i.e., 14% *versus* 2.8% for ThT and 26.1% *versus* 1.4% for BTA-1). The fact that there are more binding sites available in the grooves on the β-sheet surface than at the two ends of the β-sheet further suggests that binding in the grooves rather than at the fibril ends is the primary recognition mode of amyloid fibrils by ThT and BTA-1. This binding scheme was also observed in the study of another amyloid dye—CR[34] binding to fibrils of the amylin fragment (NFGAIL). In the case of ThT, the left double ring with the positively charged nitrogen tends to lay parallel with the β-sheet surface, exposing the positively charged nitrogen to the solvent (ThT_a and ThT_b in Fig. 4). This arrangement avoids a

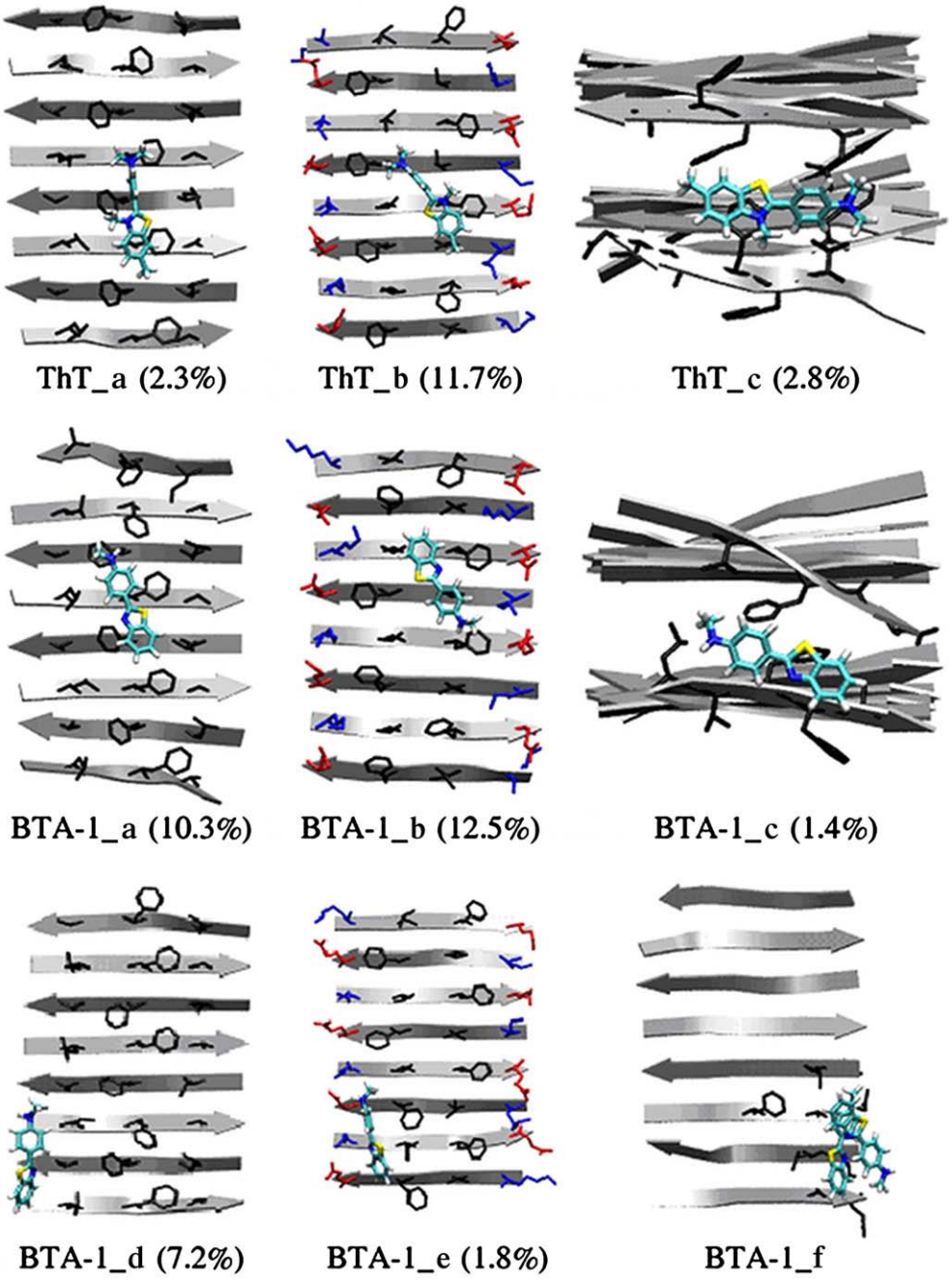

Fig. 4. Binding sites of ThT and BTA-1 to the protofibril. (a) Binding in the central groove of the lower sheet layer. (b) Binding in the central groove of the upper sheet layer. (c) Binding at the ends of the two-layer β-sheet. (d) Binding in the side grooves of the lower sheet layer. (e) Binding in the side grooves of the upper sheet layer. The aggregated abundance of the supercluster over the total population (bound + unbound) shown in parentheses is the sum over the clusters in each binding mode (e.g., ThT_a: A1–A3 in Fig. S1). (f) Dimer formation by lateral stacking. For a protofibril, only the surface side chains (blue, positively charged; red, negatively charged; and black, hydrophobic) are shown in (a), (b), (d), and (e), and only the side chains in contact with a ThT/BTA-1 molecule are shown in (c) and (f). Atoms C, N, S, and H of the dye are shown in cyan, blue, yellow, and white, respectively.

desolvation penalty upon binding and enhances Phe ring–ring interactions. In contrast, when this charge is removed in BTA-1, the left double ring becomes capable of inserting into the side groove (BTA-1_d in Fig. 4). In sum, hydrophobic interactions and Van der Waals interactions that help improve the fit of the dye into the protofibril grooves contribute to the enhanced fibril recognition by BTA-1 over ThT.

To gain a more quantitative understanding of the binding differences between ThT and BTA-1, we evaluated the binding energies at each binding site using the molecular mechanics generalized Born/surface area (MM-GBSA) method as described in Materials and Methods. These energies, averaged from the representative structures shown in Figs. S1 and S2, are listed in Table 2. Each binding site is

Table 2. MM-GBSA binding energies (in kilocalories per mole) at the different sites for each dye

Ligand	Site A[a]	Site B[b]	Site C[c]	Site D[d]	Site E[e]
ThT	−8.5±3.5	−2.2±3.1	−4.9±0.9	–	–
BTA-1	−24.3±3.5	−14.1±4.8	−16.2	−7.6±3.3	−29.2

See Fig. 4.
[a] Central grooves of the lower sheet layer.
[b] Central grooves of the upper sheet layer.
[c] Two ends of the β-sheet.
[d] Side grooves of the lower sheet layer.
[e] Side grooves of the upper sheet layer.

seen to have different binding energies/enthalpies. Assuming that the binding entropies are similar in each case, these energies correspond to different binding free energies. The three binding sites for ThT have binding energies ranging from approximately −2.2 kcal/mol to approximately −8.5 kcal/mol. The lowest binding energy (−8.5 kcal/mol) corresponds to binding in the central grooves [F4–; –F4] formed by the Phe rings of the lower sheet layer. In the case of BTA-1, the binding energies of the five binding sites range from approximately −7.6 to −29.2 kcal/mol. Interestingly, BTA-1 and ThT do not share the same strongest binding site. The site with the highest binding affinity for BTA-1 is in the side grooves formed by [K1–V3; E7–F5] of the upper sheet layer, while that for ThT is located at [F4–; –F4]. This observation may explain why BTA-1 interacts non-competitively with fibril-induced ThT fluorescence when the two dyes are tested in a competitive binding experiment to $A\beta_{40}$ fibrils.[14,24]

To compare the experimentally determined overall dissociation constants of ThT and BTA-1 to the protofibril (Table 1), we averaged the binding energy over all sites (Table 3). The binding energy of ThT to the protofibril is approximately −4.3 kcal/mol, as compared with the more favorable binding of −16.3 kcal/mol in the case of BTA-1. The relative binding free energy difference between BTA-1 and ThT is approximately −12.0 kcal/mol (assuming similar binding entropy), which is qualitatively consistent with the experimental number of approximately −3 kcal/mol.[17,20,24] The overestimation of this number seen in simulation is likely a result of approximations used in the MM-GBSA approach. Decomposition of the binding free energy into different components reveals that the solvation part

Table 3. Averaged binding energies (in kilocalories per mole) of ThT and its neutral analog BTA-1

Ligand	ΔE_{gas}[a]	ΔE_{sur}[b]	ΔE_{GB}[c]	ΔE_{tot}[d]
ThT	−23.2±10.0	−1.7±0.2	20.7±9.8	−4.3±3.6
BTA-1	−16.5±7.2	−1.6±0.6	1.9±5.4	−16.3±8.1
Change ($\Delta\Delta E$)	6.7	0.1	−18.8	−12.0

[a] Change of potential energy in gas phase upon complex formation.
[b] Change of energy due to SA change upon complex formation.
[c] Change of GB reaction field energy upon complex formation.
[d] Change of potential energy in water upon complex formation ($\Delta E_{gas} + \Delta E_{GB} + \Delta E_{sur}$).

Table 4. Calculated solvation free energies (in kilocalories per mole) of the dyes

	ΔG_{solv}		
Ligand	Electrostatics	Van der Waals	Total[a]
$ThT^+ + Cl^-$	−84.6	−6.3	−78.3±0.3
BTA-1	−5.8	−0.5	−5.3±0.2
Change ($\Delta\Delta G$)	–	–	−73.0

[a] Errors were calculated by using three blocks of trajectories (3–4, 4–5, and 5–6 ns).

(GB energy) contributes the most (approximately −18.8 kcal/mol) to the binding energy difference between BTA-1 and ThT. Hence, removing the charge from ThT to form BTA-1 significantly favors binding by decreasing the desolvation penalty upon binding (i.e., increasing hydrophobicity).

The absolute solvation free energies of $ThT + Cl^-$ and its neutral derivative BTA-1 were calculated by thermodynamic integration (TI) as described in Materials and Methods. The lipophilicity/hydrophobicity of BTA-1 is seen to be significantly improved in comparison with ThT, as indicated by the change in solvation free energy in water from −78.3 kcal/mol for $ThT + Cl^-$ to −5.3 kcal/mol for BTA-1 (Table 4). This is consistent with the experimental observation that BTA-1 is 600-fold more lipophilic than ThT.[14]

Discussion and Conclusions

Fluorescent dyes (ThT, CR, and their derivatives) are agents commonly used to identify the presence of amyloid aggregates *in vitro* and *in vivo*.[13,35–37] These dyes undergo a shift in their excitation spectrum when bound to protein and peptide aggregates but not when bound to monomers. This shift is associated with binding to the β-sheets of the aggregates, but the precise location of the binding sites on the aggregates is not experimentally known.

The objectives of this work were to elucidate the binding sites of ThT and its neutral analogy BTA-1 on amyloid protofibrils and fibrils and to determine the structure–activity relationship, in terms of solubility and binding affinity, upon mutating ThT to BTA-1. We considered a model system consisting of a protofibril of the $A\beta_{16–22}$ (KLVFFAE) peptide, the smallest aggregating fragment of the Alzheimer's disease Aβ peptide. Fibrils of this peptide exhibit all the signatures of amyloid fibrils, including a cross-β structure and staining by ThT.

Our simulations revealed multiple binding sites for the two dyes at two types of locations (two binding modes): (1) type I, in the (side and central) grooves of the β-sheet surface along the β-sheet extension direction, and (2) type II, at the ends of the β-sheet. These two types of binding sites are generic for any amyloid fibril. For the first type, the grooves arise from the repetition, along the β-sheet extension direction, of the small regular concave and convex surfaces of an extended β-strand. The sur-

face pattern of an extended β-strand is due to the alternation of side-chain directions along the backbone of an extended β-strand. The density of this type of binding sites is high, because it is proportional to the SA of exposed β-sheet in the protofibril (which typically contains one to four layers of β-sheets). This type of binding mode (type I) is consistent with the one first proposed by Krebs *et al.*[4] and subsequently by other groups.[6,8] In contrast, the site density of the second type of binding mode is low, because although the β-sheet is made of a very large number of β-strands (~100–10,000), it clearly has two ends only. The larger site density in the first type of binding site is suggestive that binding on the β-sheet surface is the dominant binding mode for the amyloid dyes. This mode explains why such linear amyloid dyes as ThT, CR, and their derivatives can bind to any amyloid fibril. Amyloid fibrils all possess a cross-β structure, regardless of the primary sequence of the protein or peptide constituting the fibrils. The linear grooves seen in amyloid fibrils are cross-β sheet specific and are rarely seen in normal ordered proteins and nonamyloid protein aggregates.

For the type I mode, multiple subtypes of binding sites can occur, as the grooves are not identical (Fig. 4). Their local chemical environment in the context of an amyloid fibril depends on the exposed side-chain types of the β-strands, on the registry (parallel, antiparallel, or mixed) between the neighboring β-strands, on the stacking between the β-sheets for forming a protofilament, and on the association of protofilaments for forming a fibril. Hence, the local chemical environment determines the binding specificity of a type of amyloid dye for a particular type of amyloid fibril. A given type of amyloid dye could only have access to a subset of all the possible grooves of a particular fibril,[8] while a different type of amyloid dye could have access to a different subset of the grooves of this same fibril type. In the case of the simple antiparallel β-sheet of the $A\beta_{16–22}$ peptide protofibril studied here, ThT is seen to bind to two types of central grooves with a large binding affinity difference (−6.3 kcal/mol between site A and site B in Fig. 4). With a small chemical modification to form BTA-1 from ThT, BTA-1 binds to two additional types of side grooves (sites D and E in Fig. 4). We note that some regular grooves could be modulated by docked irregular peptides and/or defects in the β-sheet, as suggested by experimental[38,39] and molecular dynamics[40] studies.

A recent experimental study[25] provides evidence for three distinct binding sites for the ThT class of amyloid dyes on the $A\beta_{40}$ fibrils, with stoichiometries of these sites to the Aβ peptide of 1:300, 1:4, and 1:35, respectively (Table 1). The experimental binding affinities of ThT on the three sites are ~1610 nM, ~6000 nM (1:6),[24] and ~750 nM, respectively, while those of BTA-1 are ~19.5 nM, ND (not determined), and ~200 nM, respectively. While the details of the protofibril structures are different for $A\beta_{40}$ and $A\beta_{16–22}$ [there is an additional β-strand (A30–V39) and the two β-strands form a "U" shape with parallel registry in $A\beta_{40}$, as opposed to the antiparallel registry in $A\beta_{16–22}$ fibrils], the binding modes seen in our simulations are generic to the β-sheets found in all amyloid structures. In both $A\beta_{40}$ and $A\beta_{16–22}$ fibrils, the 16–22 KLVFFAE segment is in a β-strand configuration as part of a β-sheet. Our simulations hence allowed us to identify the experimentally determined binding sites. Based on stoichiometry and the fact that we saw a large enhancement (approximately −10 kcal/mol) of the binding energy upon changing ThT to BTA-1 in our simulations (the same trend as the experimental ~80-fold increase in binding affinity change), we assigned binding at the ends of the β-sheet (mode C in Fig. 4) to the low-density site (1:300) (type II binding mode). Similarly, we assigned the grooves (side grooves and central grooves) on the same sheet layer to the high-density sites (1:4 or 1:35) (type I binding mode). These grooves correspond to hydrophobic pockets located in close proximity. This is consistent with the inference (based on the increase of intrinsic fluorescence of the dyes upon binding and additional fluorescence energy transfer studies) that the two high-density sites seen in experiment correspond to adjacent or partially overlapped sites in hydrophobic pockets.[25] Solid-state NMR studies by Petkova *et al.*[27] indicated that the Aβ fibrils possess two such hydrophobic β-sheet regions, with the first located between residue 17 and residue 21 (as in the $A\beta_{16–22}$ fibril) and the second located between residue 30 and residue 40. It is hence likely that in the context of the full-length Aβ peptide, the type I binding mode corresponds to binding at the hydrophobic grooves of sheets 17–21 and 30–40. (Our unpublished preliminary results of the binding of ThT to the full Aβ protofibril confirm this binding mode).

Our simulations were performed at an effective concentration below the critical micellar concentration of ThT. Our simulations show that ThT can bind in a monomeric form, in agreement with the work of Krebs *et al.*[4] In one of our simulations, BTA-1 bound to the fibril as a dimer (Fig. 4f), a scenario consistent with the work of Groenning *et al.*,[5,6] with a mechanism involving the initial binding of the monomer followed by the binding of a second BTA-1 monomer. Khurana *et al.*[7] reported atomic force microscopy (AFM) measurements in which 3-nm micelles of ThT were seen bound to amyloid fibrils. Because their experiments were performed at ~4 μM,[7] well below the critical micellar concentration of ~35 μM,[8] it is unlikely that the micelles bound in a preformed manner to the fibril. Our simulations rather suggest that the AFM experiments may be explained as follows: Binding to the fibrils would occur with ThT in a monomeric form. This would be followed by lateral stacking of additional ThT molecules to the bound ThT to form an oligomer with a height of 3 nm containing up to seven monomers (the thickness of a ThT is ~4.3 Å). The rotation of the ThT molecules along the lateral axis (Fig. 4f) leads to a circular shape consistent with the circular two-dimensional projections

observed in AFM experiments. The formation of such a bound aggregate would occur for a lower concentration of ThT than in the bulk and more rapidly, due to the reduction in mobility of ThT upon binding to the β-sheet surface (i.e., reducing the entropic barrier for further association). Our proposed mechanism, in which initial monomer binding can be followed by stacking of other ThT molecules, offers an alternative explanation for the fluorescence enhancement of ThT. This new picture unifies previously proposed mechanisms (namely, enhanced fluorescence via reduction of the internal motion of monomeric ThT by binding to the grooves[4] of the fibril, excimer formation by ThT dimerization,[5,6] and hydrogen bonding of a ThT micelle[7] to the fibril).

Our simulation results might also shed light on the structural feature of early Aβ oligomers. These oligomers are increasingly believed to play a critical role in the pathology of Alzheimer's disease, but little is known about the structure of these early aggregates. Recent studies[41,42] show that ThT and CR analogs detect Aβ oligomers *in vitro* and *in vivo* and, based on binding ratio and affinity, that these oligomers may have the same two types of binding sites as the Aβ$_{40}$ fibrils.[41] Since our simulations indicate that the two binding modes correspond to binding to the β-sheets of the fibrils, they implicitly suggest that the oligomers also have a certain degree of β-sheet structure. In other words, the conformational transition from a random coil to an extended β-sheet might already be partially completed in the oligomers. Further study on oligomerization is required to clarify this issue.

Finally, the structure–activity relationship upon mutating ThT to BTA-1 in terms of solubility and binding affinity was studied. With removal of the charge on ThT, BTA-1 remained quite soluble in water as indicated by the favorable solvation free energy of −5.3 kcal/mol, but its hydrophobicity was nonetheless significantly increased by 73.0 kcal/mol (Table 4), leading to a higher tendency to form small oligomers (such as the dimer seen in our simulations). In terms of binding, it is interesting to note that the positively charged ThT bound to hydrophobic and aromatic residues rather than to negatively charged residues, indicating that the ring–ring and hydrophobic interactions, rather than the salt bridges, are the stabilizing forces for ligand binding. Indeed, with removal of the charge and a methyl group of ThT, the overall binding energy of BTA-1 increased by approximately −16 kcal/mol in the MM-GBSA calculation, which is in qualitative agreement with experimental measurements (approximately −3 kcal/mol). In addition, shape complementarity (ligand + groove) is an additional factor contributing to stabilizing binding as evidenced by the fact that BTA-1 has stronger binding affinity (20 nM) than neutral BTA-2 and BTA-0 (140 and 30 nM, respectively), which have two methyl groups and no methyl group, respectively, connecting to the aniline nitrogen[14] (Fig. 1, left side of ligand). In other words, two methyl groups might block the insertion of the dye into the shallow grooves, but the complete absence of methyl groups would in turn weaken the hydrophobic interaction—with both scenarios resulting in weaker binding affinities than in the case of BTA-1. As a general rule, amyloid dyes have a linear structure, and our simulations are consistent with a mechanism in which this linear structure facilitates their fit in the linear grooves of amyloid fibrils.

In conclusion, the simulations presented here have provided detailed information about the properties of amyloid dyes and their binding to β-sheet-enriched amyloid aggregates, augmenting our knowledge from experimental studies.

Materials and Methods

System preparation

Our binding simulation system consisted of a 16-peptide oligomer (representing a protofibril), four ligand molecules, and ~9100 water molecules, with an additional four chloride ions in the case of the positively charged ThT (IDs 5 and 6 in Table 5). The 16-peptide oligomer was constructed from the 7-residue Aβ$_{16–22}$ peptide fragment (*N*-acetyl-KLVFFAE-NH_2) arranged in a double-layered β-sheet structure. Each layer consists of eight in-register antiparallel β-strands, the arrangement suggested by solid NMR experiments.[11,12] The two layers could be stacked in parallel or antiparallel fashion, with the interlayer hydrophobic core formed between the hydrophobic residues from the upper layer and the lower layer, respectively, in three ways: [–V–F–; –V–F–], [–L–F–A–; –L–F–A–], and

Table 5. Simulated systems

ID	Content	No. of water molecules	Box dimensions (Å^3)	Ligand concentration (mM)	No. of simulations	Length of each (ns)
1	$ThT^+ + Cl^-$	–	–	–	2×12 λ[a]	6
2	$ThT^+ + Cl^-$	771	33×33×33	–	2×12 λ[a]	6
3	BTA-1	–	–	–	2×12 λ[a]	6
4	BTA-1	597	31×31×31	–	2×12 λ[a]	6
5	Protofibril[b] + $4ThT^+ + 4Cl^-$	9106	97×75×58	15.7	4	20
6	Protofibril[b] + 4BTA-1	9096	99×75×57	15.7	4	20

[a] The TI simulations were conducted with 12 λ windows for Gaussian integration to obtain the solvation free energy. Set 1, electrostatic interaction; set 2, LJ interaction; λ = {0.00922 0.99078 0.04794 0.95206 0.11505 0.88495 0.20634 0.79366 0.31608 0.68392 0.43738 0.56262}.
[b] The protofibril consists of two β-sheets stacked in parallel, each composed of 8 Aβ$_{16–22}$ peptides in antiparallel registry, for a total of 16 peptides.

[–V–F–; –L–F–A–].[43] The parallel arrangement with the mixed interface pattern [–V–F–; –L–F–A–] was shown to form stable and well-aligned aggregates in a previous simulation study[43] and was used in this study (Fig. 2a). This construct has the additional advantage of enabling the simultaneous study of binding of the amyloid dyes to the two types of β-sheet surfaces (Fig. 2b and c). The dimensions of the peptide oligomer were ~70×25×20 Å^3 in the directions of β-sheet extension (main-chain hydrogen bond), β-sheet stacking (perpendicular to the β-sheet surface), and β-strand, respectively. Four dye molecules were initially placed ~10 Å away from the 16-peptide oligomer along two directions: the β-sheet extension and β-sheet stacking directions (two molecules for each direction). In the case of ThT, four negative chloride ions (Cl^-) were added to neutralize the four negative charges carried by the four ThT molecules. The solute molecules were immersed into a rectangular box of ~9100 water molecules with dimensions of 97×75×58 Å^3. The periodic water box was constructed in such a way that the solute was at least ~8 Å away from the box surface and the minimum distance between the solute and the image was ~16 Å. The apparent concentrations of dye molecule and the peptide oligomer were ~15.7 and ~3.9 mM, respectively, but the effective concentrations were much lower due to the small number of molecules in the periodic box in the simulations. We estimate the effective concentration of ThT to be below the critical micelle concentration of 35 μM, which is likely why no ThT oligomer was formed in the simulations. The advantage of using four dye molecules in each simulation system is that it allows sampling of four conformations in a single trajectory and thus enhances sampling in comparison with systems with a single dye molecule (i.e., 4 simulations on a system with four dye molecules are equivalent to 16 simulations a system with one dye molecule).[44]

Duan *et al.*'s all-atom point-charge force field[45] (AMBER ff03) was chosen to represent the peptide. The solvent was explicitly represented by the TIP3P[46] water model. The parameters for ThT were obtained from a previous study.[34] Following the same protocol, we developed the parameters for BTA-1 as follows: after geometry optimization at the HF/6-31G* level, the partial charges were derived by fitting to the gas-phase electrostatic potential calculated at the HF/6-31G* level of quantum mechanical theory using the RESP (restrained electrostatic potential) method[47] and other force parameters of BTA-1 molecule were taken from the AMBER GAFF[48] parameter set. The parameter files in AMBER format are available upon request.

Binding simulations

The AMBER 8 simulation package[48] was used in both molecular dynamics simulations and data processing. The ligand–protofibril–water system was subjected to periodic boundary conditions via both minimum image and discrete Fourier transform as part of the particle-mesh Ewald method.[9] After the initial energy minimization, a total of eight simulations (four runs for each dye) was performed with different initial random velocities. The initial velocities were generated according to the Maxwell–Boltzmann distribution at 500 K. The simulations started after a 10.0-ps run at 500 K to randomize the orientations and positions of the four dye molecules. A short 1.0-ns molecular dynamics simulation at 320 K in the NPT ensemble (constant pressure and temperature) was performed to adjust system size and density and to equilibrate the solvent. The simulations were continued at 320 K for 19 ns in the NVT ensemble (constant volume and temperature). The elevated temperature (10 K higher than 37 °C) was used in the simulations to enhance the hydrophobic effect. Particle-mesh Ewald method[9] was used to treat the long-range electrostatic interactions. SHAKE[49] was applied to constrain all bonds connecting hydrogen atoms, and a time step of 2.0 fs was used. In order to reduce the computation, we calculated nonbonded forces using a two-stage RESPA (reversible reference system propagator algorithm) approach[50] in which the forces within a 10-Å radius were updated every step and those beyond 10 Å were updated every two steps. Temperature was controlled at 320 K using Berendsen *et al.*'s algorithm[51] with a coupling constant of 2.0 ps. The center-of-mass translation and rotation were removed every 500 steps. Studies have shown that this removes the "block of ice" problem.[52,53] The trajectories were saved at 2.0-ps intervals for further analysis. The strategy of using higher-solute concentration and elevated temperature (320 K) as in this study has successfully been exploited previously to reduce the computational cost associated with simulating peptide association[54–56] and ligand binding.[44] The combined reduction in the computational cost due to the elevation of concentration of ligand and protein is expected to be close to 6 orders of magnitude ($10^3 \times 10^3$). Nonetheless, 32 Opteron (2.2 GHz) CPUs were used for ~40 days to complete the eight binding simulations.

Solvation free energy calculation

The calculation of the solvation free energy of a ligand was broken down into the two steps shown in Fig. 5: (1) mutation of a ligand in gas phase into a dummy molecule by turning off nonbonded interactions [electrostatic and Lennard–Jones (LJ) interactions] within the ligand and (2) mutation of the ligand in water into a dummy molecule by turning off the nonbonded interactions between the water molecules and the ligand, as well as within the ligand. For each step, two sets of parallel calculations were done to get the electrostatic and LJ parts of the free energy. The electrostatic interactions were turned off by removing the partial charges on the ligand, and the LJ interactions were turned off by using the λ-dependent soft-core (SC) potential implemented in AMBER 10,[57]

$$V_{SC} = 4\varepsilon(1-\lambda)\left\{\frac{1}{\left[\alpha\lambda + (r/\sigma)^6\right]^2} - \frac{1}{\alpha\lambda + (r/\sigma)^6}\right\} \quad (1)$$

in which ε is well depth, σ is interatomic distance at zero LJ potential, r is the interatomic distance, and α is an adjustable constant set to 0.5 in this study. The pertur-

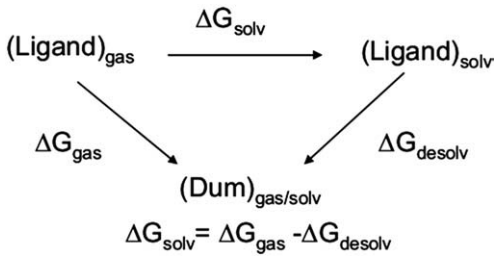

Fig. 5. Thermocycle used to calculate the absolute solvation free energy.

bation ($\lambda = 0 \rightarrow 1$) started from full nonbonded interactions ($\lambda = 0$) and ended at null nonbonded interactions ($\lambda = 1$), and each set of calculations consisted of 12 λ windows (Table 5). The free energy change was obtained by TI with Gaussian integration scheme over 12 λ windows.[58] The free energy change is given by the expression:

$$\Delta G_{TI} = \int_0^1 \left\langle \frac{\partial V(\lambda)}{\partial \lambda} \right\rangle_\lambda d\lambda = \sum_{i=1}^{12} W_i \left\langle \frac{\partial V(\lambda)}{\partial \lambda} \right\rangle_\lambda \quad (2)$$

where the angular brackets denote an ensemble average, using $V(\lambda)$ as the potential, and W_i is the weight in Gaussian integration. The simulation protocol is the same as the one in the binding simulation except for a few differences: the solvated simulations were done in an NPT ensemble; a Langevin thermostat[59] with a collision frequency of 2 ps^{-1} was employed to keep the system temperature at 310 K. To keep the system neutral in the perturbation, we calculated the solvation free energy of ThT plus its counter ion (Cl^-) instead.

Clustering analysis

To gain a clearer understanding of the binding interactions, we grouped the bound complexes into different structural clusters based on the RMSD of the dye molecule (cutoff of 5 Å) after aligning the protofibril.[44] A representative structure (the centroid) of the top 15 abundant clusters from the combined four simulation runs for each dye is shown in Figs. S2 and S3. In the second level of clustering, the clusters having the same binding site regardless of dye pose are further merged into a supercluster (Fig. 4).

Binding energy calculation

A binding site is identified from the abovementioned two-level clustering analysis. The binding energy of a dye molecule to the protofibril in each site (Fig. 4) was evaluated on the centroids of the multiple structural clusters contained in a supercluster using the MM-GBSA module[60] in AMBER package in which the solvation free energy is represented by the GB term (the polar part of the solvation) and an SA term (the apolar part of the solvation free energy). Although the MM-GBSA calculations may overestimate the absolute binding free energy due to missing entropic terms (e.g., translation, rotation, and conformational entropy change of the solute upon binding), they usually give a reasonable estimate of the relative binding free energy when the entropic changes of two binding sites are comparable.[60,61] We attempted to calculate the binding free energies using the more accurate TI method, but this method showed significant convergence problems associated with the large size of the complex systems studied.

Acknowledgements

This project was funded by the David and Lucile Packard Foundation, the National Science Foundation (MCB 0642086 to J.S.E.), and the National Institutes of Health (AG027818 to M.B.). Computer time was provided by the genbeo cluster of the UC Davis Genome Center and the lonestar cluster of the Texas Advanced Computing Center (LRAC MCA 05S027). We thank Dr. Thomas Steinbrecher for providing the code on soft-core potential and Dr. Catherine Carpenter for helping format the manuscript.

Supplementary Data

Supplementary data associated with this article can be found, in the online version, at doi:10.1016/j.jmb.2008.09.062

References

1. Chiti, F. & Dobson, C. M. (2006). Protein misfolding, functional amyloid, and human disease. *Annu. Rev. Biochem.* **75**, 333–366.
2. Dobson, C. M. (2004). Principles of protein folding, misfolding and aggregation. *Semin. Cell Dev. Biol.* **15**, 3–16.
3. Furumoto, S., Okamura, N., Iwata, R., Yanai, K., Arai, H. & Kudo, Y. (2007). Recent advances in the development of amyloid imaging agents. *Curr. Top. Med. Chem.* **7**, 1773–1789.
4. Krebs, M. R. H., Bromley, E. H. C. & Donald, A. M. (2005). The binding of thioflavin-T to amyloid fibrils: localisation and implications. *J. Struct. Biol.* **149**, 30–37.
5. Groenning, M., Olsen, L., van de Weert, M., Flink, J. M., Frokjaer, S. & Jorgensen, F. S. (2007). Study on the binding of thioflavin T to β-sheet-rich and non-β-sheet cavities. *J. Struct. Biol.* **158**, 358–369.
6. Groenning, M., Norrman, M., Flink, J. M., van de Weert, M., Bukrinsky, J. T., Schluckebier, G. & Frokjaer, S. (2007). Binding mode of thioflavin T in insulin amyloid fibrils. *J. Struct. Biol.* **159**, 483–497.
7. Khurana, R., Coleman, C., Ionescu-Zanetti, C., Carter, S. A., Krishna, V., Grover, R. K. *et al.* (2005). Mechanism of thioflavin T binding to amyloid fibrils. *J. Struct. Biol.* **151**, 229–238.
8. Sabate, R., Lascu, I. & Saupe, S. (2008). On the binding of thioflavin-T to HET-s amyloid fibrils assembled at pH2. *J. Struct. Biol.* **162**, 387–396.
9. Essmann, U., Perera, L., Berkowitz, M. L., Darden, T. A., Lee, H. & Pedersen, L. G. (1995). A smooth particle mesh Ewald method. *J. Chem. Phys.* **103**, 8577–8593.
10. De Felice, F. G., Vieira, M. N. N., Saraiva, L. M., Figueroa-Villar, J. D., Garcia-Abreu, J., Liu, R. *et al.* (2004). Targeting the neurotoxic species in Alzheimer's disease: inhibitors of Aβ oligomerization. *FASEB J.* **18**, 1366–1372.
11. Balbach, J. J., Ishii, Y., Antzutkin, O. N., Leapman, R. D., Rizzo, N. W., Dyda, F. *et al.* (2000). Amyloid fibril formation by Aβ(16–22), a seven-residue fragment of the Alzheimer's β-amyloid peptide, and structural characterization by solid state NMR. *Biochemistry*, **39**, 13748–13759.
12. Petkova, A. T., Buntkowsky, G., Dyda, F., Leapman, R. D., Yau, W. M. & Tycko, R. (2004). Solid state NMR reveals a pH-dependent antiparallel β-sheet registry in fibrils formed by a β-amyloid peptide. *J. Mol. Biol.* **335**, 247–260.
13. LeVine, H. (1999). Quantification of β-sheet amyloid fibril structures with thioflavin T. In *Amyloid, Prions, and Other Protein Aggregates* (Wetzel, R., ed.), vol. 309, pp. 274–284, Academic Press, San Diego, CA.

14. Klunk, W. E., Wang, Y. M., Huang, G. F., Debnath, M. L., Holt, D. P. & Mathis, C. A. (2001). Uncharged thioflavin-T derivatives bind to amyloid-β protein with high affinity and readily enter the brain. *Life Sci.* **69**, 1471–1484.
15. Mathis, C. A., Wang, Y. M., Holt, D. P., Huang, G. F., Debnath, M. L. & Klunk, W. E. (2003). Synthesis and evaluation of C-11-labeled 6-substituted 2-arylbenzothiazoles as amyloid imaging agents. *J. Med. Chem.* **46**, 2740–2754.
16. Mathis, C. A., Holt, D. P., Wang, Y., Huang, G. F., Debnath, M. L. & Klunk, W. E. (2001). A lipophilic C-11-labeled derivative of thioflavin-T for amyloid assessments in Alzheimer's disease. *J. Nucl. Med.* **42**, 113P.
17. Mathis, C., Holt, D., Wang, Y. M., Huong, G. F., Debnath, M. & Klunk, W. (2002). Evaluation of a potent thioflavin-T analog for *in vivo* imaging of amyloid with PET. *Neurobiol. Aging*, **23**, S349.
18. Mathis, C. A., Holt, D. P., Wang, Y., Huang, G. F., Debnath, M. L. & Klunk, W. E. (2002). F-18-labeled thioflavin-T analogs for amyloid assessment. *J. Nucl. Med.* **43**, 166P.
19. Mathis, C. A., Wang, Y., Huang, G. F., Holt, D. P., Debnath, M. L. & Klunk, W. E. (2002). Radioiodinated thioflavin-T derivative for imaging amyloid. *J. Nucl. Med.* **43**, 359P.
20. Mathis, C. A., Bacskai, B. J., Kajdasz, S. T., McLellan, M. E., Frosch, M. P., Hyman, B. T. *et al.* (2002). A lipophilic thioflavin-T derivative for positron emission tomography (PET) imaging of amyloid in brain. *Bioorg. Med. Chem. Lett.* **12**, 295–298.
21. Mathis, C., Holt, D., Wang, Y. M., Huang, G. F., Debnath, M. & Klunk, W. (2004). Development of thioflavin-T analogs for amyloid imaging with PET. *Neurobiol. Aging*, **25**, 248.
22. Mathis, C., Holt, D., Wang, Y. M., Huang, G. F., Debnath, M. & Klunk, W. (2004). Evaluation of a potent thioflavin-T analog for *in vivo* imaging of amyloid with PET. *Neurobiol. Aging*, **25**, 248–249.
23. Pike, K. E., Savage, G., Villemagne, V. L., Ng, S., Moss, S. A., Maruff, P. *et al.* (2007). β-amyloid imaging and memory in non-demented individuals: evidence for preclinical Alzheimer's disease. *Brain*, **130**, 2837–2844.
24. Levine, H. (2005). Multiple ligand binding sites on Aβ(1–40) fibrils. *Amyl. J. Prot. Fold. Dis.* **12**, 5–14.
25. Lockhart, A., Ye, L., Judd, D. B., Merritt, A. T., Lowe, P. N., Morgenstern, J. L. *et al.* (2005). Evidence for the presence of three distinct binding sites for the thioflavin T class of Alzheimer's disease PET imaging agents on β-amyloid peptide fibrils. *J. Biol. Chem.* **280**, 7677–7684.
26. Buchete, N. V., Tycko, R. & Hummer, G. (2005). Molecular dynamics simulations of Alzheimer's β-amyloid protofilaments. *J. Mol. Biol.* **353**, 804–821.
27. Petkova, A. T., Ishii, Y., Balbach, J. J., Antzutkin, O. N., Leapman, R. D., Delaglio, F. & Tycko, R. (2002). A structural model for Alzheimer's β-amyloid fibrils based on experimental constraints from solid state NMR. *Proc. Natl Acad. Sci. USA*, **99**, 16742–16747.
28. Gnanakaran, S., Nussinov, R. & Garcia, A. E. (2006). Atomic-level description of amyloid β-dimer formation. *J. Am. Chem .Soc.* **128**, 2158–2159.
29. Favrin, G., Irback, A. & Mohanty, S. (2004). Oligomerization of amyloid Aβ(16–22) peptides using hydrogen bonds and hydrophobicity forces. *Biophys. J.* **87**, 3657–3664.
30. Klimov, D. K., Straub, J. E. & Thirumalai, D. (2004). Aqueous urea solution destabilizes Aβ(16–22) oligomers. *Proc. Natl Acad. Sci. USA*, **101**, 14760–14765.
31. Nguyen, P. H., Li, M. S., Stock, G., Straub, J. E. & Thirumalai, D. (2007). Monomer adds to preformed structured oligomers of Aβ-peptides by a two-stage dock–lock mechanism. *Proc. Natl Acad. Sci. USA*, **104**, 111–116.
32. Ma, B. Y. & Nussinov, R. (2002). Stabilities and conformations of Alzheimer's β-amyloid peptide oligomers (Aβ(16–22′) Aβ(16–35′) and Aβ(10–35)): sequence effects. *Proc. Natl Acad. Sci. USA*, **99**, 14126–14131.
33. Soto, P., Griffin, M. A. & Shea, J. E. (2007). New insights into the mechanism of Alzheimer amyloid-β fibrillogenesis inhibition by *N*-methylated peptides. *Biophys. J.* **93**, 3015–3025.
34. Wu, C., Wang, Z. X., Lei, H. X., Zhang, W. & Duan, Y. (2007). Dual binding modes of Congo red to amyloid protofibril surface observed in molecular dynamics simulations. *J. Am. Chem .Soc.* **129**, 1225–1232.
35. Levine, H. (1995). Thioflavine-T interaction with amyloid β-sheet structures. *Amyl. Int. J. Exp. Clin. Invest.* **2**, 1–6.
36. Klunk, W. E., Pettegrew, J. W. & Abraham, D. J. (1989). Quantitative evaluation of Congo red binding to amyloid-like proteins with a β-pleated sheet conformation. *J. Histochem. Cytochem.* **37**, 1273–1281.
37. Klunk, W. E., Jacob, R. F. & Mason, R. P. (1999). Quantifying amyloid β-peptide (Aβ) aggregation using the Congo red Aβ (CR-Aβ) spectrophotometric assay. *Anal. Biochem.* **266**, 66–76.
38. Wetzel, R. (2002). Ideas of order for amyloid fibril structure. *Structure*, **10**, 1031–1036.
39. Esler, W. P., Stimson, E. R., Jennings, J. M., Vinters, H. V., Ghilardi, J. R., Lee, J. P. *et al.* (2000). Alzheimer's disease amyloid propagation by a template-dependent dock–lock mechanism. *Biochemistry*, **39**, 6288–6295.
40. Takeda, T. & Klimov, D. K. (2008). Temperature-induced dissociation of Aβ monomers from amyloid fibril. *Biophys. J.* **95**, 1758–1772.
41. Maezawa, I., Hong, H., Liu, R., Wu, C., Cheng, R. H., Kung, M. *et al.* (2008). Congo red and thioflavin-T analogs detect Aβ oligomers. *J. Neurochem.* **104**, 457–468.
42. Chimon, S. & Ishii, Y. (2005). Capturing intermediate structures of Alzheimer's β-amyloid, Aβ(1–40), by solid-state NMR spectroscopy. *J. Am. Chem .Soc.* **127**, 13472–13473.
43. Rohrig, U. F., Laio, A., Tantalo, N., Parrinello, M. & Petronzio, R. (2006). Stability and structure of oligomers of the Alzheimer peptide Aβ(16–22): from the dimer to the 32-mer. *Biophys. J.* **91**, 3217–3229.
44. Wu, C., Lei, H., Wang, Z. X., Zhang, W. & Duan, Y. (2006). Phenol red interacts with the protofibril-like oligomers of an amyloidogenic hexapeptide NFGAIL through both hydrophobic and aromatic contacts. *Biophys. J.* **91**, 3664–3672.
45. Duan, Y., Chowdhury, S., Xiong, G., Wu, C., Zhang, W., Lee, T. *et al.* (2003). A point-charge force field for molecular mechanics simulations of proteins based on condensed-phase QM calculations. *J. Comput. Chem.* **24**, 1999–2012.
46. Jorgensen, W. L., Chandrasekhar, J., Madura, J. D., Impey, R. W. & Klein, M. L. (1983). Comparisons of simple potential functions for simulating liquid water. *J. Chem. Phys.* **79**, 926–935.
47. Bayly, C. I., Cieplak, P., Cornell, W. D. & Kollman, P. A. (1993). A well-behaved electrostatic potential-based method using charge restraints for deriving atomic charges—the RESP model. *J. Phys. Chem.* **97**, 10269–10280.
48. Wang, J. M., Wolf, R. M., Caldwell, J. W., Kollman, P. A. & Case, D. A. (2004). Development and testing

of a general amber force field. *J. Comput. Chem.* **25**, 1157–1174.
49. Ryckaert, J. P., Ciccotti, G. & Berendsen, H. J. C. (1977). Numerical integration of the cartesian equations of motion of a system with constraints: molecular dynamics of *n*-alkanes. *J. Chem. Phys.* **23**, 327–341.
50. Procacci, P. & Berne, B. J. (1994). Multiple time scale methods for constant pressure molecular dynamics simulations of molecular systems. *Mol. Phys.* **83**, 255–272.
51. Berendsen, H. J. C., Postma, J. P. M., van Gunsteren, W. F., DiNola, A. & Haak, J. R. (1984). Molecular dynamics with coupling to an external bath. *J. Chem. Phys.* **81**, 3684–3690.
52. Chiu, S. W., Clark, M., Subramaniam, S. & Jakobsson, E. (2000). Collective motion artifacts arising in long-duration molecular dynamics simulations. *J. Comput. Chem.* **21**, 121–131.
53. Harvey, S. C., Tan, R. K. Z. & Cheatham, T. E. (1998). The flying ice cube: velocity rescaling in molecular dynamics leads to violation of energy equipartition. *J. Comput. Chem.* **19**, 726–740.
54. Wu, C., Lei, H. & Duan, Y. (2004). Formation of partially-ordered oligomers of amyloidogenic hexapeptide (NFGAIL) in aqueous solution observed in molecular dynamics simulations. *Biophys. J.* **87**, 3000–3009.
55. Wu, C., Lei, H. & Duan, Y. (2005). The role of Phe in the formation of well-ordered oligomers of amyloidogenic hexapeptide (NFGAIL) observed in molecular dynamics simulations with explicit solvent. *Biophys. J.* **88**, 2897–2906.
56. Wu, C., Lei, H. & Duan, Y. (2005). Elongation of ordered peptide aggregate of an amyloidogenic hexapeptide (NFGAIL) observed in molecular dynamics simulations with explicit solvent. *J. Am. Chem. Soc.* **127**, 13530–13537.
57. Steinbrecher, T., Mobley, D. L. & Case, D. A. (2007). Nonlinear scaling schemes for Lennard–Jones interactions in free energy calculations. *J. Chem. Phys.* **127**.
58. Hummer, G. & Szabo, A. (1996). Calculation of free-energy differences from computer simulations of initial and final states. *J. Chem. Phys.* **105**, 2004–2010.
59. Chandrasekhar, S. (1943). Stochastic problems in physics and astronomy. *Rev. Mod. Phys.* **15**, 1–89.
60. Kollman, P. A., Massova, I., Reyes, C., Kuhn, B., Huo, S., Chong, L. *et al.* (2000). Calculating structures and free energies of complex molecules: combining molecular mechanics and continuum models. *Acc. Chem. Res.* **33**, 889–897.
61. Gilson, M. K. & Zhou, H. X. (2007). Calculation of protein–ligand binding affinities. *Annu. Rev. Biophys. Biomol. Struct.* **36**, 21–42.